STM JOURNALS

Journal of
Offshore Structure and Technology

ISSN: 2349-8986
Volume 12, Issue 2, 2025
May–August
DOI (Journal): 10.37591/JoOST

https://journals.stmjournals.com/joost

Research JoOST

Turbulence Exploitation in Offshore Wind Farms: Improvement in Generated Power

Carlos Armenta-Déu*

Abstract

The limited space available for wind energy projects highlights the importance of improving the efficiency of wind farms, like the exploitation of turbulent wakes. In this work, we analyze the available energy associated with the turbulent wakes generated by offshore wind turbines at various downstream distances using a computational fluid dynamics (CFD) program (Autodesk). Classical wind conditions for offshore wind farms are established for the probability distribution of wind speed, applying the Weibull distribution, and for the angular distribution of wind direction, using the Von Mises distribution. This study allows determining the amount of recovered energy by the drag turbine at different downstream distances, resulting in an efficiency increase up to 11.59% for a drag turbine with a diameter of 80 m and an estimated power coefficient of C_p=0.15 located at a downstream distance of 2.5 times the diameter of the conventional wind turbine.

Keywords: Turbulent fluid, wakes, CFD technique, modelling and simulation, offshore wind turbine, efficiency improvement

INTRODUCTION

The rotational wakes' analysis is critical for an efficient wind farm design because of the horizontal axis wind turbine (HAWT) operational mode, depending on the lift force created by the interaction between the wind and the wind turbine blade. Lift forces are optimal if the wind turbine operates under a laminar flow regime, forcing it to separate two adjacent wind turbines at a minimum distance equivalent to the one where the rotational wake vanishes; at this point, the turbulent kinetic energy associated with the rotational wake becomes null [1–3].

The rotational wakes' study derives from solving the Navier-Stokes equations because the system operates under unsteady turbulent regime, where numerical solution does not apply. To do so, we use the Computational Fluid Dynamic (CFD) technique through the turbulent k-ε model, based on the turbulent kinetic energy; in this way, we obtain a wind speed distribution along the rotational wake development, and the turbulent kinetic energy evolution [4–7].

***Author for Correspondence**
Carlos Armenta-Déu
E-mail: cardeu@ucm.es

Professor, Department of Matter Structure, Thermal Physics and Electronics, Faculty of Physical Sciences, Complutense University of Madrid, Madrid, Spain

Received Date: May 06, 2025
Accepted Date: May 25, 2025
Published Date: June 10, 2025

Citation: Carlos Armenta-Déu. Turbulence Exploitation in Offshore Wind Farms: Improvement in Generated Power. Journal of Offshore Structure and Technology. 2025; 12(2): 22–35p.

The CFD Autodesk software supports the rotational wake development analysis, comparing the results with the Jensen 2D model to validate the methodological procedure. This model is widely used in wind resource models like WASP and WindPRO [8–15]. On the other hand, we compare the generated energy by a conventional wind turbine operating under lift or drag force, since in turbulent wind regimes the drag force is significant. The comparative analysis uses the combined probability from Weibull and Von Mises distributions, calculating the energy from the CFD simulation results for identical operating conditions.

Every wind park design requires a detailed study and analysis, including wind resource evaluation, environmental and economic viability, visual impact, and onsite terrain geological prospection. All these factors merge into a point before starting the wind farm building; therefore, it is critical for efficient land use since the space is limited [16–18]. We distinguish two marine area types in offshore wind farms: the priority use zone (PUZ) and the high potential use zone (PAZ). PUZ are for global interests, requiring specific areas, while PAZ are for sectorial activities where the future possible use is a priority; among the PAZ, we can mention the wind farms [19–24].

This research work studies the performance improvement in offshore wind farms by optimizing marine space use. To do so, we analyze the turbulent wake evolution aiming to insert drag force wind turbines. The consequence is an incrsease in the output power generation and global efficiency.

THEORETICAL FOUNDATIONS

Considering that the wind circulates through a virtual cylindrical tube (control volume) with no interaction with the surrounding air, the wind flow is constant. The upstream control volume (CV) has a cylindrical shape of identical diameter to the wind rotor. Nevertheless, due to the interaction between incoming wind flow and rotor blades, the tube expands, increasing its diameter and reducing the speed according to the Bernoulli's equation (Figure 1); therefore [25]:

$$U_D = U_\infty (1-a); U_W = U_\infty (1-2a) \tag{1}$$

U is the wind speed, and subscripts D, ∞, and W account for wind rotor position and upstream and downstream flow. The parameter a is the fluent factor.

Using the classical expression for the wind power, the wind turbine efficiency, C_p, is [25]:

$$C_p = 4a(1-a)^2 \tag{2}$$

Considering the air density constant throughout the Control Volume, applying the Bernoulli's equation to a turbulent regime wind flow, we obtain the rotational wake surface factor, F, as in Eq. (3):

$$F = 1 - \frac{A_\infty}{A_W} = 1 - \frac{U_W}{U_\infty} \tag{3}$$

Combining Eqs. (1)–(3):

$$C_p = \left[1.5 + \frac{1}{2}(1-F) - 4(1-F)^2 + 2(1-F)^3\right]^3 \tag{4}$$

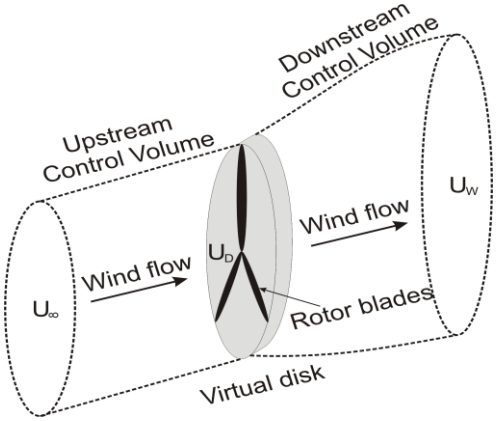

Figure 1. Schematic view of the wind flow circulation.

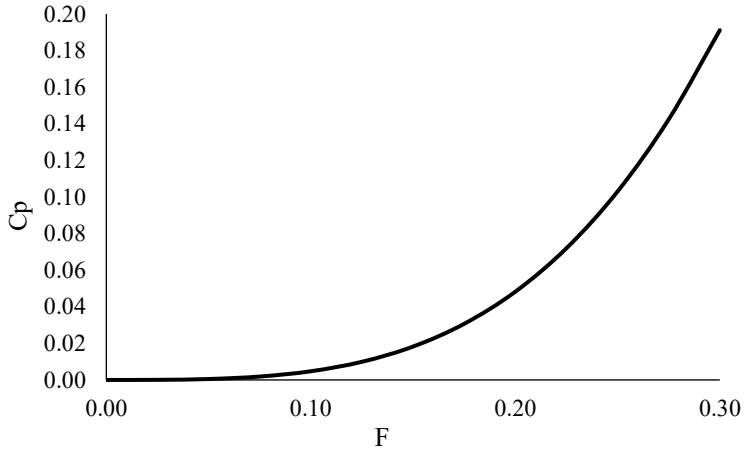

Figure 2. Wind turbine power coefficient evolution with rotational wake surface factor.

The *F*-factor depends on how much turbulent kinetic energy absorbs the air from the rotational wake; a zero value for the *F*-factor means that air does not absorb turbulent kinetic energy, and the rotational wake remains unchanged, generating a null value for the power coefficient *Cp*; as air absorbs turbulent kinetic energy from the rotational wake, the *F*-factor raises, and the wind flow becomes less turbulent, making the power coefficient increase. If we represent the power coefficient versus the *F*-factor, we observe how *Cp* increases with *F*, achieving the optimum value for an *F*-factor equal to 0.3 (Figure 2).

The above simulation matches experimental values corresponding to wind turbines operating with turbulent flows like the Savonius wind turbine, whose power coefficient is C_p=0.15, on average, when working under drag force mode [26, 27].

The turbulent flow mathematical analysis requires the Navier-Stokes application since no numerical solution applies [28–31]; therefore, the interaction between wind and blade due to drag forces results in the following analytical expressions:

$$\begin{aligned}
\rho\frac{Du}{Dt} &= \frac{\partial}{\partial x}\left(-p+\tau_{xx}\right)+\frac{\partial}{\partial y}\left(\tau_{xy}\right)+\frac{\partial}{\partial z}\left(\tau_{xz}\right)+S_{Mx}\\
\rho\frac{Dv}{Dt} &= \frac{\partial}{\partial x}\left(\tau_{xy}\right)+\frac{\partial}{\partial y}\left(-p+\tau_{yy}\right)+\frac{\partial}{\partial z}\left(\tau_{yz}\right)+S_{My}\\
\rho\frac{Dw}{Dt} &= \frac{\partial}{\partial x}\left(\tau_{xz}\right)+\frac{\partial}{\partial y}\left(\tau_{yz}\right)+\frac{\partial}{\partial z}\left(-p+\tau_{zz}\right)+S_{Mz}
\end{aligned} \tag{5}$$

u, v, and *w* are the three wind speed Cartesian components, ρ is the air density, *D* is the material derivative function, *p* is the air pressure, and τ is the shear stress tensor due to viscous effects. Subscripts *x, y,* and *z* correspond to the three space directions. The parameter *S* represents the mass force; if only gravity applies, $S_{Mx}=S_{My}=0$, and $S_{Mz}=-\rho g$.

For Newtonian fluids, the shear stress tensor becomes [32]:

$$\begin{aligned}
&\tau_{xx}=2\mu\frac{\partial u}{\partial x};\ \tau_{yy}=2\mu\frac{\partial v}{\partial y};\ \tau_{zz}=2\mu\frac{\partial w}{\partial z}\\
&\tau_{xy}=\tau_{yx}=\mu\left[\frac{\partial u}{\partial y}+\frac{\partial v}{\partial x}\right];\ \tau_{xz}=\tau_{zx}=\mu\left[\frac{\partial u}{\partial z}+\frac{\partial w}{\partial x}\right];\ \tau_{yz}=\tau_{zy}=\mu\left[\frac{\partial v}{\partial z}+\frac{\partial w}{\partial y}\right]
\end{aligned} \tag{6}$$

Combining Eqs. (5) and (6), and grouping terms:

$$\rho \frac{D}{Dt}\left(U_j\right) = -\frac{\partial p}{\partial j} + \nabla\left(\mu \nabla U_j\right) + \left[s_{Mj}\right] \rightarrow j = x, y, z \tag{7}$$

First term in Eq. (7) represents the convective change rate of momentum in the x direction. The term describes how fluid motion develops along the wake generated by the turbine blades. Second term represents the forces due to the pressure gradient in the x direction. In the case of rotating wakes, these pressure gradients are fundamental for describing how the pressure varies around the wake and how this variation influences the flow distribution. Third term describes the effects of viscosity and momentum diffusion along the wake. Air viscosity plays a crucial role in the wake energy dissipation, as it influences the smoothing of velocities and the distribution of turbulence in the rotational flow, directly affecting the stability and structure of the wake, determining how it develops and diffuses as it moves away from the rotor. Last term is a correction term representing an additional source like external forces, compressibility effects, or interaction between phases.

The Jensen model

The Jensen model is a Gaussian speed profile based on the speed deficit coefficient U/U_∞ [33–35]. This coefficient accounts for the rotational wake-to-free upstream wind speed ratio. Mathematically:

$$\frac{U}{U_\infty} = 1 - C(x)\exp\left[-\frac{r^2}{2\sigma_w^2(x)}\right] \tag{8}$$

$C(x)$ is the normalized downstream wind speed, r is the distance to the rotor axis, and $\sigma_w(x)$ is the Gaussian distribution standard deviation.

The Jensen model imposes the following premises:

- The inlet wind flow is incompressible, steady-state, and non-viscous.
- The wind rotor is thickness null; the wind force acts uniformly on every surface point.
- Any infinitesimal flow has the same pressure as the inlet flow.

Applying Bernoulli's equation, and imposing a linear rotational wake expansion ($r_w \approx 2\sigma_w$), we obtain:

$$\frac{U}{U_\infty} = 1 - A(x)\exp\left[-\frac{2}{\left(kx/r_a + 1\right)^2}\left(\frac{r}{r_a}\right)^2\right] \tag{9}$$

k is the rotational wake damping coefficient, r_a is the rotor radius, and $A(x)$ is a function depending on the thrust coefficient, C_T, as in:

$$A(x) = \frac{2\left(1 - \sqrt{1 - C_T}\right)}{\left(kx/r_a + 1\right)^2} \tag{10}$$

Wind Distribution

The analysis of the turbulent kinetic energy associated to the rotational wake implies the knowledge of the wind distribution. In our study, we use a combination of the Weibull and Von Mises distribution to evaluate the wind speed probability [36–41]. Figure 3 shows the Weibull and Von Mises probability density function.

Weibull distribution responds to a mathematical function of the type:

$$f_D(U) = \frac{\kappa}{\lambda}\left(\frac{U}{\lambda}\right)^{\kappa - 1}\exp\left[-\left(\frac{U}{\lambda}\right)^{\kappa}\right] \tag{11}$$

λ is the blade tip linear velocity.
For the Von Mises distribution:

$$f_V(\theta,\mu,\kappa)=\frac{1}{2\pi I_o(\kappa)}\exp\left[\kappa\cos\left(\theta-\mu\right)\right] \tag{12}$$

θ is the wind direction, μ is the average angular direction, representing the predominant wind direction, κ is the concentration parameter, equivalent to the inverse of the normal distribution variance, and $I_o(\kappa)$ is the modified Bessel function of the first type and order zero.

The analysis for the simulation results in Figure 3 shows a predominant wind direction at 225º and a most probable wind speed of 8 m/s.

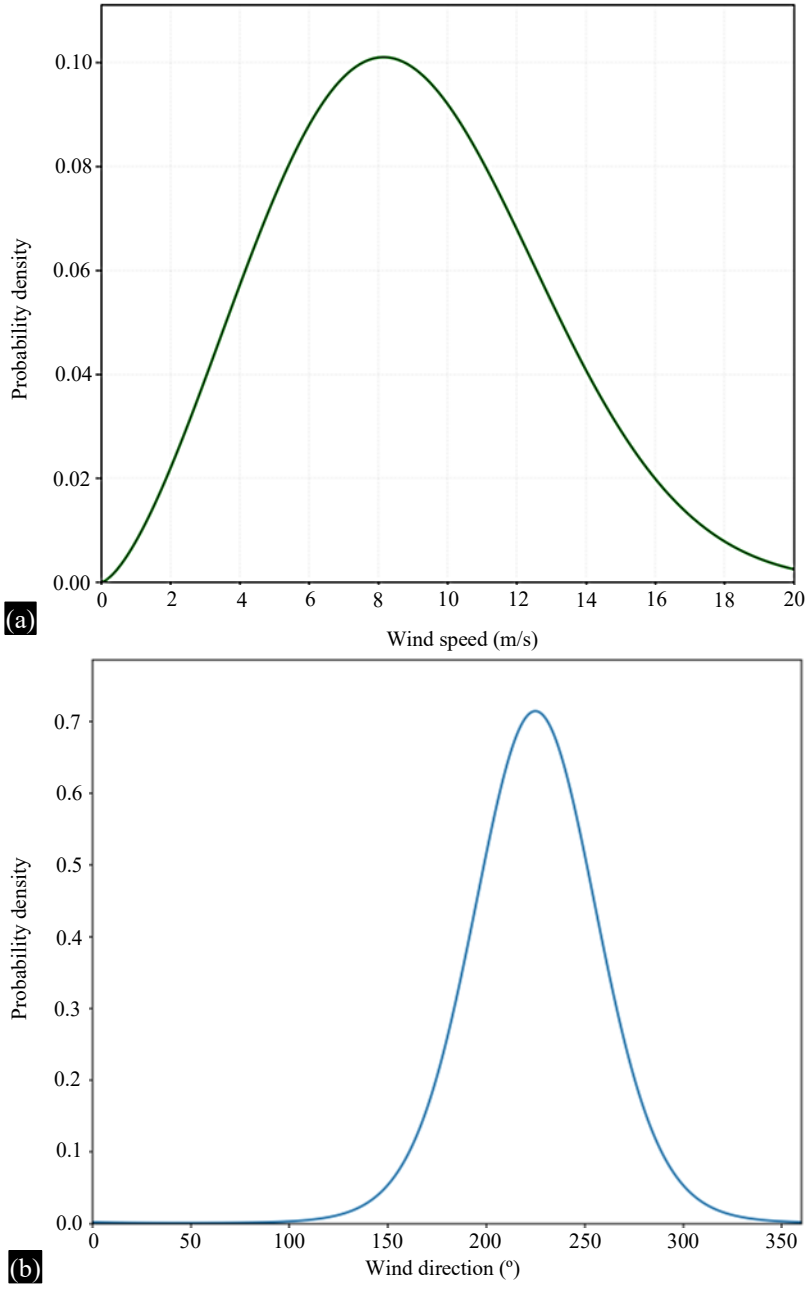

Figure 3. (a) Left: Weibull probability density for λ=10 m/s and κ=2.5; (b) Right: Von Mises probability density for κ=2.5 and μ=225º [42].

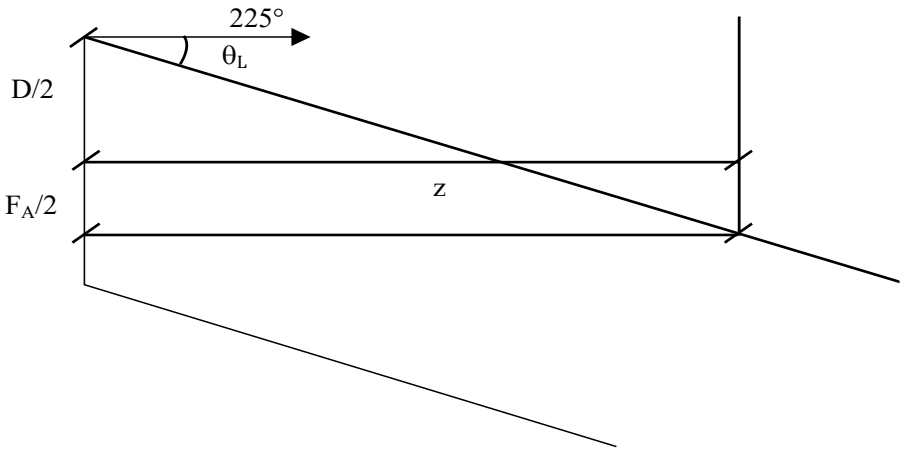

Figure 4. Schematic view of geometric distribution of conventional and drag force wind turbines.

TURBULENT KINETIC ENERGY

Since we intend to use the turbulent kinetic energy for power generation in drag force wind turbines, it is necessary to evaluate the rotational wake turbulent kinetic energy recovery fraction [43–46]. To this goal, we apply the Mean Kinetic Power (MKP) expression:

$$MKP = \frac{1}{2}\rho U^3 A_R \tag{13}$$

A_R is the wind rotor area.

Analogously, for the Turbulent Kinetic Power (TKP), we have:

$$TKP = TKE\,\rho U A_R \tag{14}$$

The term TKE expresses the turbulent kinetic energy.

If we insert a drag force wind turbine between two conventional turbines in a wind farm, the θ angle is limited by the layout geometry (Figure 4).

D_A and D are the rotor diameter for the drag force and conventional wind turbine, and z is the distance between them.

According to the Figure 3 drawing:

$$\theta_L = \arctan\left(\frac{D_A + D}{2z}\right) \tag{15}$$

The calculation considers that the rotational wake and the conventional wind turbine rotor have equivalent diameter.

Beyond the θ_L point the wind flow becomes laminar; therefore, the drag force wind turbine operates with turbulent flow within the range μ-θ_L<θ<μ+θ_L.

The collected annual energy is:

$$\xi_{annual} = \sum_i 8760\, f_{D,i}\left[\left(TKP\right)_i C_{p,D} F_p + \left(MKP\right)_i C_{p,L}\left(1 - F_p\right)\right] \tag{16}$$

f_D is the Weibull probability function, defined in Eq. (11). Subscripts D and L for the power coefficient, C_p, correspond to wind turbine operation under drag and lift force. F_p is the probability

function that rotational wake arrives at the downstream wind turbine; therefore, the term *(1-F_p)* is the probability that the downstream wind turbine operates under laminar flow. We define the F_p function as:

$$F_p = \int_{\mu-\theta_L}^{\mu+\theta_L} f_V(\theta, \mu, \kappa)\, d\theta \tag{17}$$

Considering the lift and drag force power coefficient equal, and combining Eqs. (11)–(17), we have:

$$\xi_{annual} = \sum_i 8760 \left[\frac{\kappa}{\lambda}\left(\frac{U_i}{\lambda}\right)^{\kappa-1} exp\left[-\left(\frac{U_i}{\lambda}\right)^{\kappa}\right]\right]\left[\frac{TKE\rho A_R C_p^o}{2\pi I_o(\kappa)} U_i \left(\int_{\mu-\theta_L}^{\mu+\theta_L}[exp[\kappa\, cos(\theta-\mu)]]\, d\theta\right) + \right.$$
$$\left. + \frac{1}{2}\rho A_R U_i^3 C_p^o \left(1 - \left[\frac{1}{2\pi I_o(\kappa)} \int_{\mu-\theta_L}^{\mu+\theta_L}[exp[\kappa\, cos(\theta-\mu)]]\, d\theta\right]\right)\right] \tag{18}$$

Simulation

The simulation runs for a power coefficient of C_p^o=*0.15* for the drag force wind turbine and C_p=*0.4* for the conventional one [47]. The latter value corresponds to the standard power coefficient for massive power generation wind turbines; the former value derives from Figure 2 for *F=0.28*, corresponding to the closest point to optimum operating conditions. The diameters for the lift and drag force wind turbines are *D*=110 m, and D_A=80 m. The coefficients *κ, μ*, and *λ* are the same as for the Weibull and Von Mises distributions shown in Figure 3. The *z* value is variable depending on the selected distance between lift and drag force wind turbines, expressed in terms of the conventional wind turbine rotor diameter. We adopt the standard air density value for wind farm operation, ρ=1.225 kg/m^3.

The first simulation develops for z=1D. Figure 5 shows the results for the TKP. The results analysis from Figure 5 shows that for the maximum wind speed probability, according to the Weibull distribution in Figure 3, the turbulent kinetic power (TKP) is 226 kW, corresponding to the turbulent kinetic energy average value. On the other hand, *Fp*=0.78, representing 78% of the operating time the rotational wake arrives at the downstream conventional wind turbine for *DA=D/2*=55 m. The *Fp* value derives from the area covered by the Von Mises distribution within the angular operating range (Figure 6). Repeating the simulation for z=1.5D (Figure 7).

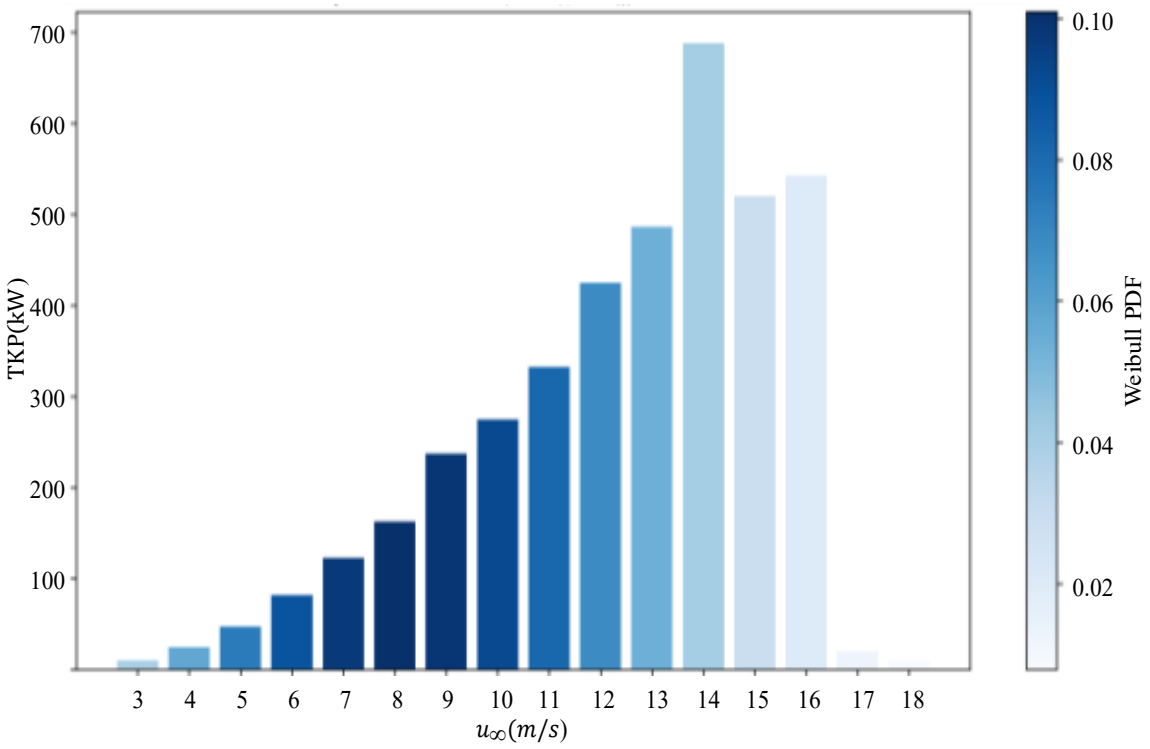

Figure 5. Simulated values for TKP at z=1D.

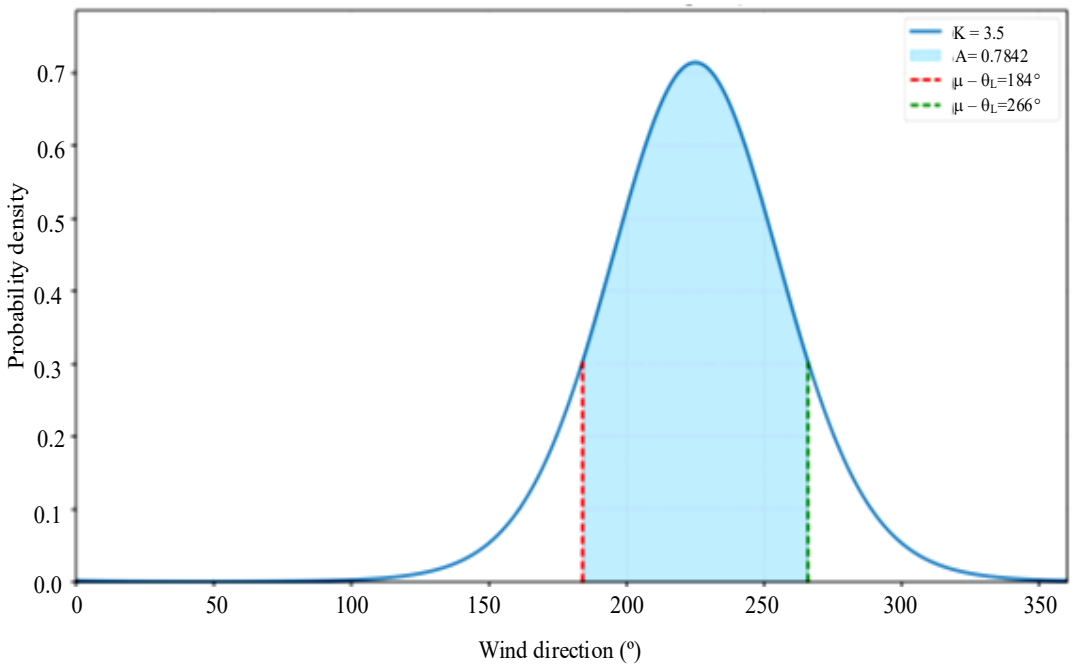

Figure 6. Von mises distribution for angular range operation at z=1D.

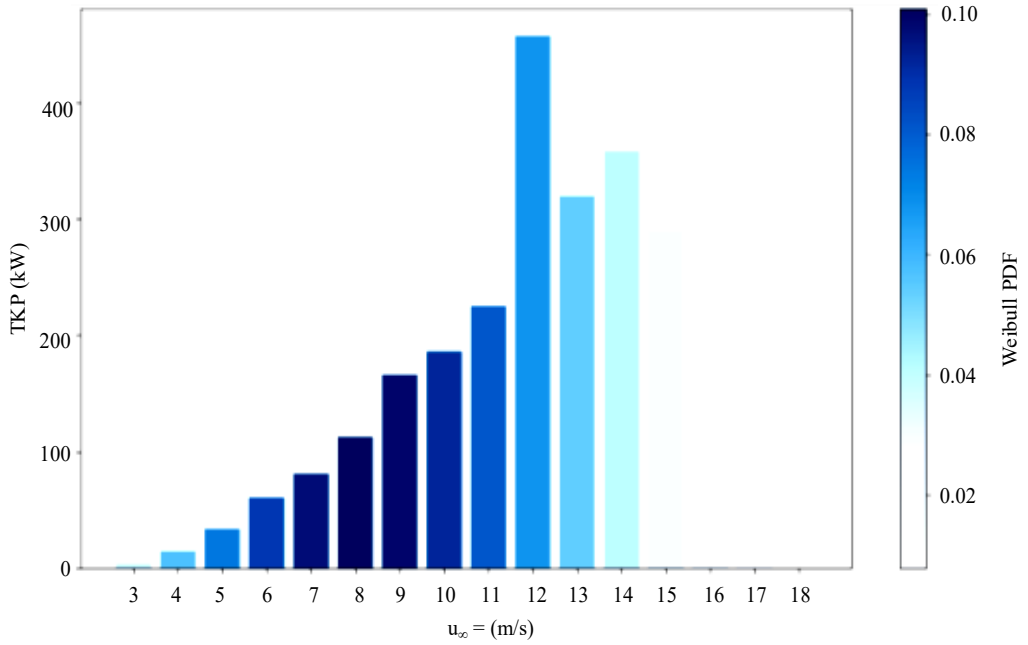

Figure 7. Simulated values for TKP at z=1.5D.

The maximum TKP value is 157.5 kW, representing a 30% reduction, regarding the previous case (z=1D). Furthermore, the *Fp* value lowers to 0.64 (Figure 8), meaning that 36% of the operating time, the drag force wind turbine operates under laminar flow.

Extending the simulation for z=2D, we have (Figure 9):

The maximum turbulent kinetic power for z=2D is 145.8 kW, 35% lower than for z=1D and 7% lower than for z=1.5D. These values show that the TKP reduction smooths as we separate from the critical distance (z=1D), where the wind turbine uses the turbulent kinetic energy at maximum efficiency.

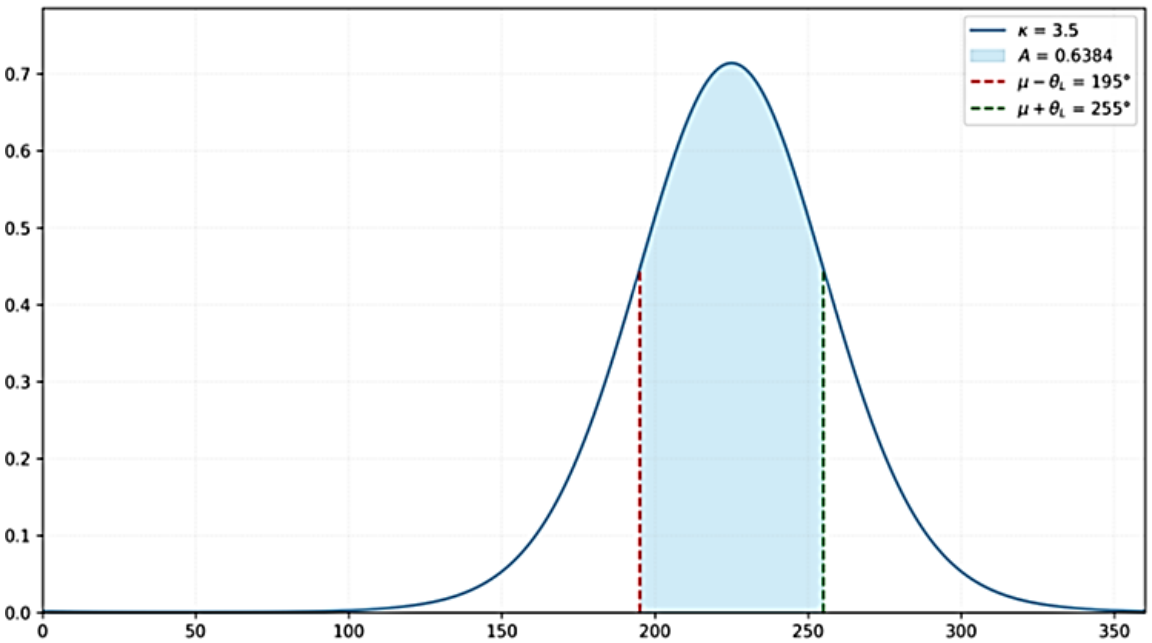

Figure 8. Von mises distribution for angular range operation at z=1.5D.

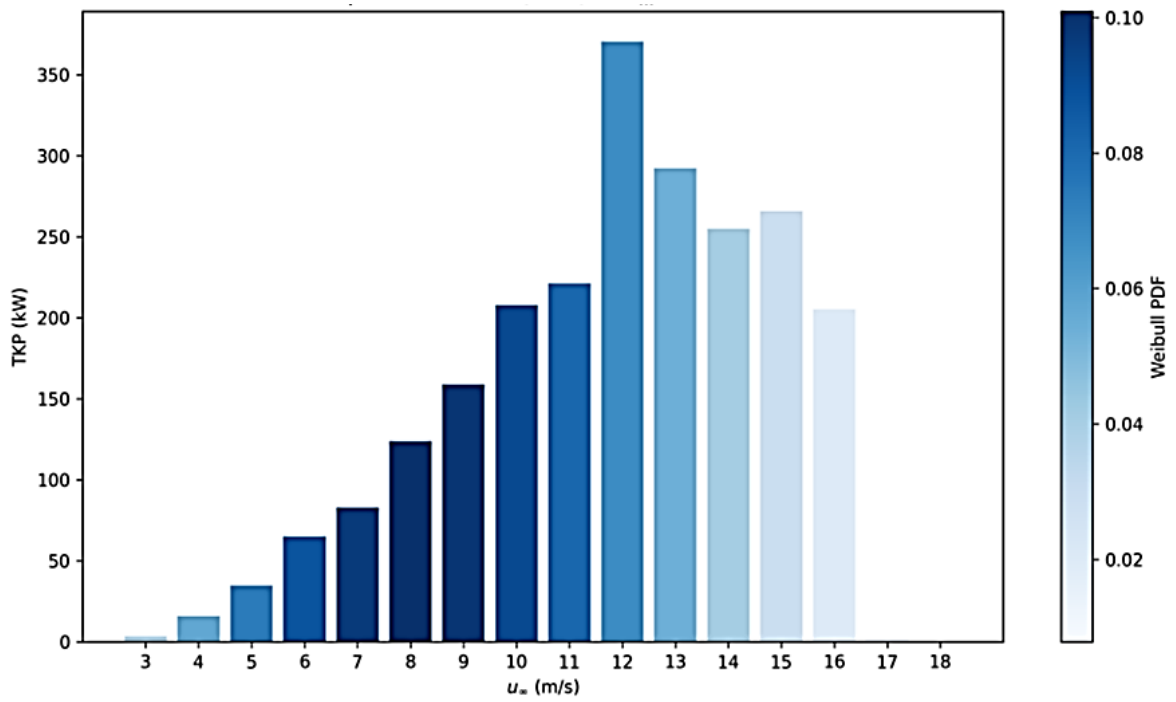

Figure 9. Simulated values for TKP at z=2D.

The F_p lowers to 0.52 (Figure 10), meaning than nearly 50% of the time the rotational wake strikes the downstream conventional wind turbine.

Finally, the simulation runs for z=2.5D, obtaining the following results (Figure 11):

The maximum turbulent kinetic power for this case is 110.4 kW, and the F_p value is 0.44.

Compiling data from the simulations and making a comparative analysis between TKP and F_p data for all cases, we have (Table 1):

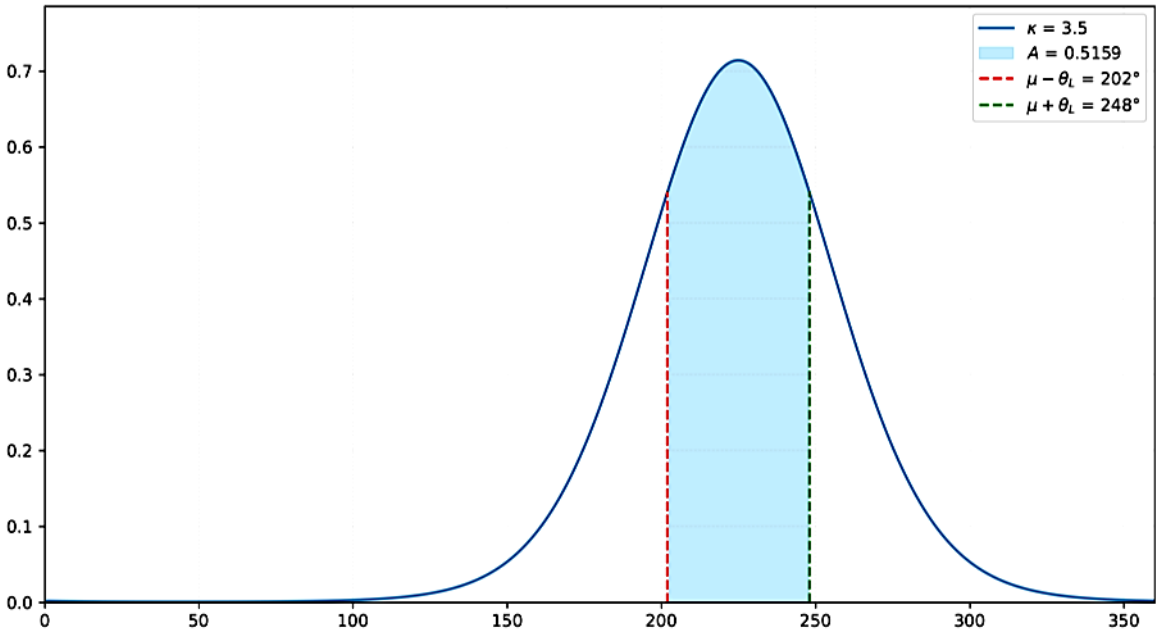

Figure 10. Von Mises distribution for angular range operation at z=2D.

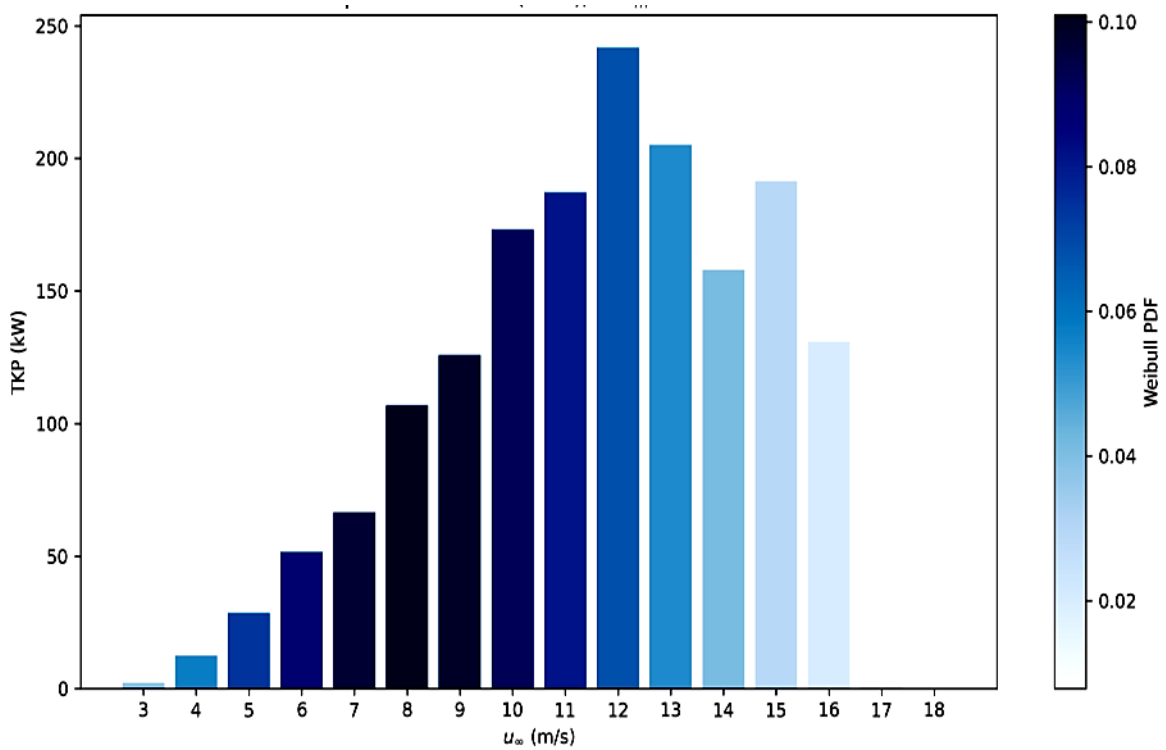

Figure 11. Simulated values for TKP at z=2.5D.

Table 1. Comparative analysis of TKP and F_p values for variable distance between conventional and drag force wind turbines.

z	1D	1.5D	2D	2.5D
TKP (kW)	226	157.5	145.8	110.4
F_p	0.78	0.64	0.52	0.44
Power reduction (%) regarding z=1D	---	30	35	51
TKP ratio	1	0.70	0.65	0.49

Correlating the TKP ratio, R_{TKP}, and the relative distance, z/D, we obtain the following third degree polynomial function with a regression coefficient R^2=1, meaning that the correlation is fully accurate.

$$R_{TKP} = -0.4749\left(\frac{z}{D}\right)^3 + 2.6398\left(\frac{z}{D}\right)^2 - 4.9499\left(\frac{z}{D}\right) + 3.785 \quad (19)$$

This polynomial function shows that turbulent kinetic power reduces with third power of relative distance, meaning that turbulent kinetic energy rapidly lowers as we move away from the conventional wind turbine that generates the rotational wake.

Calculating the MKP values from the TKP simulated data, we obtain for conventional wind turbines of 80 and 110 m diameter, operating at λ=10 m/s and κ=*2.5* (Figures 12 and 13):

RECOVERED ENERGY

Applying Eq. (18), and using data from Figure 13, for a conventional wind turbine of 110 m diameter with a power coefficient C_p=0.4, the available energy is:

$$\xi_D = 8760 C_p MKP_{m,D} = (8760)(0.4)(4610) = 16153440kWh = 16153.44MWh \quad (20)$$

Repeating the calculation for a drag force wind turbine of 80 m diameter with a power coefficient C_p=0.15, placed at a variable distance from the primary wind turbine, we have (Table 2):

Table 2. Turbulent kinetic power (kW) and annual energy (MWh/year) for variable distance between conventional and drag force wind turbine.

z	1D	1.5D	2D	2.5D
TKP (kW)	226.02	157.48	145.83	110.41
TKE (MWh/year)	232.90	132.10	98.86	63.24
Turbulent factor range (F_p)	0.78	0.64	0.52	0.44
MKE (MWh/year)	691.89	1159.35	1552.10	1808.59
Laminar factor range	0.22	0.36	0.48	0.56
Annual energy generation (MWh/year)	924.79	1291.45	1650.96	1871.83
TKE use efficiency (%)	5.73	7.99	10.22	11.59

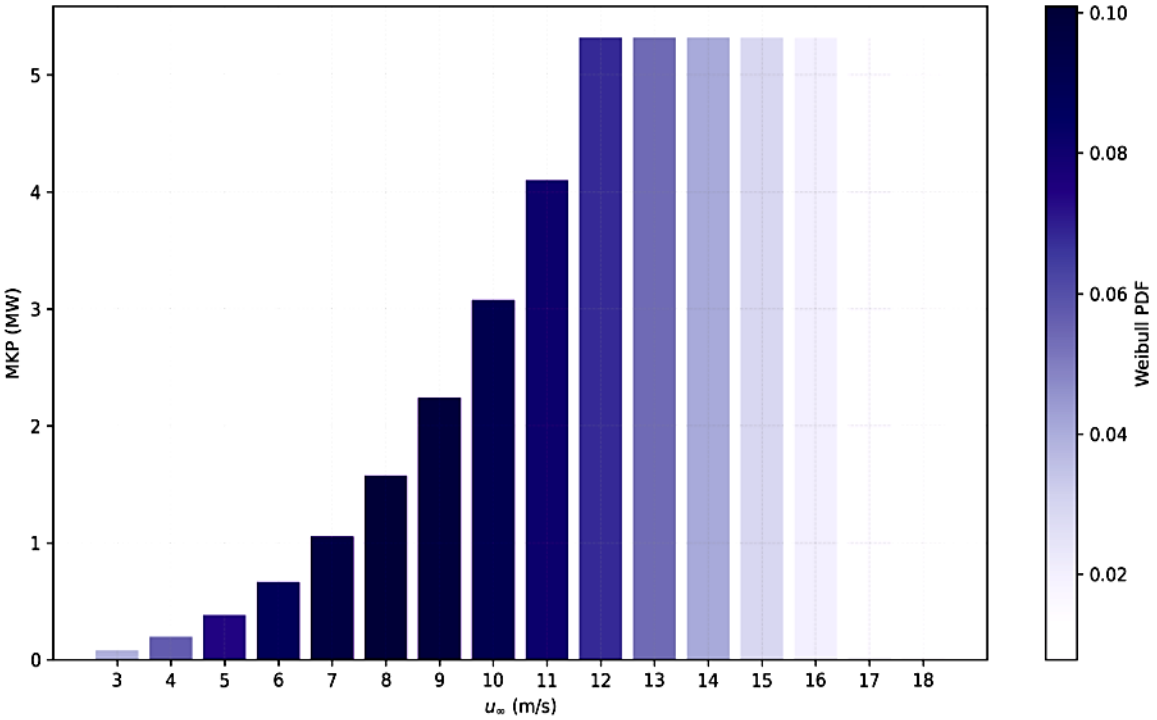

Figure 12. Estimated values for MKP for a conventional wind turbine of 80 m diameter.

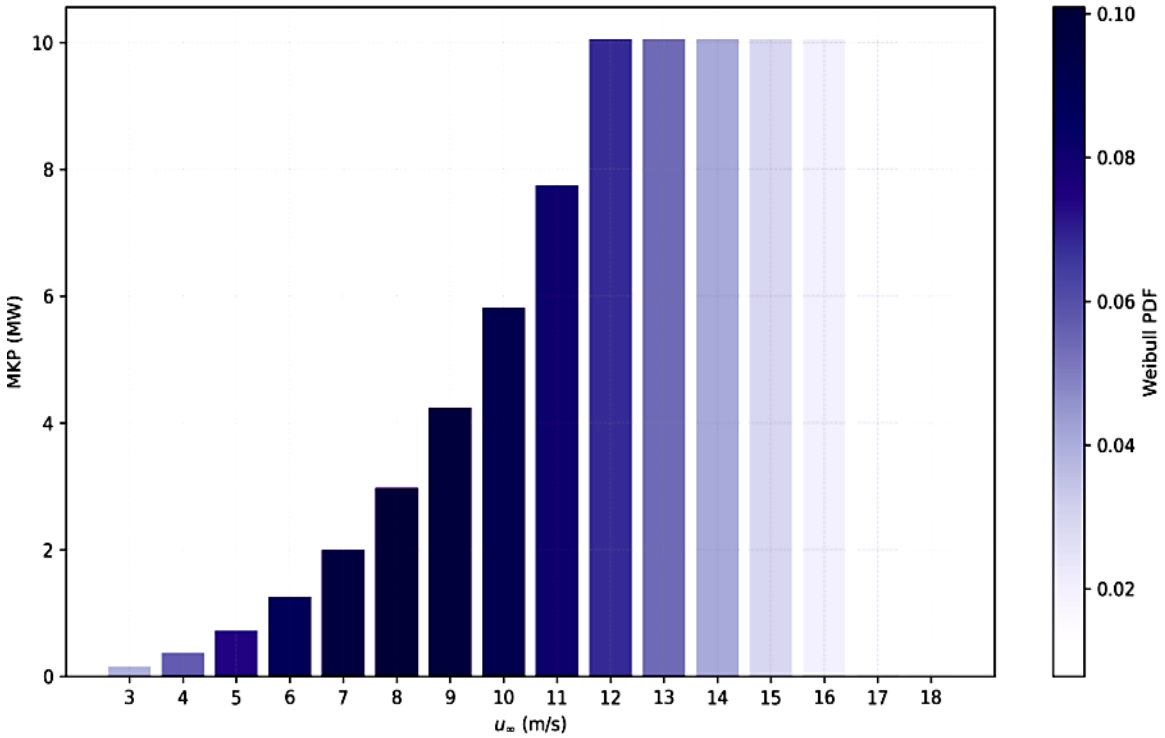

Figure 13. Estimated values for MKP for a conventional wind turbine of 110 m diameter.

CONCLUSION

This research work studies the available energy from rotational wakes generated by conventional wind turbines. The study deals with the specific case of a 110 m diameter rotor blade, representing a regular size for massive electric generation wind turbines.

The study analyzes the rotational wake probability of reaching the next wind turbine in line on a wind farm. The probability varies depending on the absorbed turbulent kinetic energy between two consecutive wind turbines. The probability decreases if we insert a drag-force wind turbine in the free space between conventional wind turbines since it absorbs a fraction of the turbulent kinetic energy the rotational wake carries.

The probability decays with the distance between the first inline conventional turbine and the drag force one, following a third-degree polynomial function with high accuracy ($R2$=1). Consequently, inserting the drag force wind turbine as far away as possible without interfering with the current operation of the second inline conventional wind turbine is more efficient. The simulation results show that inserting the drag force wind turbine at a distance of 2.5 times the diameters from the traditional wind turbine minimizes the rotational wake turbulent effects on the second-in-line wind turbine.

The study evaluates the efficiency improvement in the second-in-line conventional wind turbine as a function of the distance between the traditional first-inline and the drag force wind turbine. The study shows that the efficiency improves from a minimum of 5.73% for a distance equivalent to the diameter of the conventional wind turbine to a maximum of 11.59% for two and a half times the diameter.

REFERENCES

1. González JS, Rodríguez ÁG, Mora JC, Payán MB, Santos JR. Overall design optimization of wind farms. Renew Energy. 2011; 36(7): 1973–1982.
2. Herbert-Acero JF, Probst O, Réthoré PE, Larsen GC, Castillo-Villar KK. A review of methodological approaches for the design and optimization of wind farms. Energies. 2014; 7(11): 6930–7016.

3. Samorani M. The wind farm layout optimization problem. In Handbook of wind power systems. Berlin, Heidelberg: Springer Berlin Heidelberg; 2014; 21–38.
4. Wake BE, Sankar LN. Solutions of the Navier-Stokes Equations for the Flow About a Rotor Blade. J Am Helicopter Soc. 1989; 34(2): 13–23.
5. Persillon H, Braza M. Physical analysis of the transition to turbulence in the wake of a circular cylinder by three-dimensional Navier–Stokes simulation. J Fluid Mech. 1998; 365: 23–88.
6. Tryggeson H. Analytical vortex solutions to Navier-Stokes equation. Doctoral dissertation. Sweden: Växjö University Press; 2007.
7. Ivanell S, Sørensen JN, Mikkelsen R, Henningson D. Analysis of numerically generated wake structures. Wind Energy: An International Journal for Progress and Applications in Wind Power Conversion Technology. 2009; 12(1): 63–80.
8. Berge E, Gravdahl AR, Schelling J, Tallhaug L, Undheim O. Wind in complex terrain. A comparison of WAsP and two CFD-models. In Proceedings from EWEC. 2006 Feb; 27.
9. Makridis A, Chick J. Validation of a CFD model of wind turbine wakes with terrain effects. J Wind Eng Ind Aerodyn. 2013; 123: 12–29.
10. Travaglini R, Melani PF, Balduzzi F, Orlando S, Viti V, Bianchini A. A critical insight into the most effective CFD settings to model atmospheric stability in wind energy applications. In J Phys: Conf Ser. IOP Publishing. 2024 Jun; 2767(9): 092031.
11. Pereira R, Guedes R, Santos S. Comparing WAsP and CFD wind resource estimates for the regular user. In Proceedings of the European Wind Energy Conference, Warsaw, Poland. 2010 Apr.
12. Corbett JF, Poenario A, Horn U, Leask P. An extensive validation of CFD flow modelling. Proceedings of the DEWEK, Bremen, Germany. 2015; 18–19.
13. Sharma PK, Warudkar V, Ahmed S. Application of a new method to develop a CFD model to analyze wind characteristics for a complex terrain. Sustain Energy Technol Assess. 2020; 37: 100580.
14. Bengtsson J. Turbulence Wind Flow Modeling in Complex Terrain. A Comparison Between a Linear Model, a CFD Model and a NWP Model. Master's Thesis. Sweden: Chalmers University of Technology; 2015.
15. Bechmann A. WAsP CFD A new beginning in wind resource assessment. Technical report. Denmark: Riso National Laboratory; 2012.
16. Reddy SR. Wind Farm Layout Optimization (WindFLO): An advanced framework for fast wind farm analysis and optimization. Appl Energy. 2020; 269: 115090.
17. González JS, Rodríguez ÁG, Mora JC, Payán MB, Santos JR. Overall design optimization of wind farms. Renew Energy. 2011; 36(7): 1973–1982.
18. Chowdhury S, Zhang J, Tong W, Messac A. Modeling the influence of land-shape on the energy production potential of a wind farm site. J Energy Resour Technol. 2014; 136(1): 011203.
19. Ministerio para la transición ecológica y el reto demográfico. [Online]. https://www.miteco.gob.es/es/costas/temas/proteccion-medio-marino/ordenacion-del-espacio-maritimo.html
20. Lee AH, Chen HH, Kang HY. Multi-criteria decision making on strategic selection of wind farms. Renew Energy. 2009; 34(1): 120–126.
21. Van Haaren R, Fthenakis V. GIS-based wind farm site selection using spatial multi-criteria analysis (SMCA): Evaluating the case for New York State. Renew Sustain Energy Rev. 2011; 15(7): 3332–3340.
22. Cowell R. Wind power, landscape and strategic, spatial planning—the construction of 'acceptable locations' in Wales. Land Use Policy. 2010; 27(2): 222–232.
23. Ajanaku BA, Strager MP, Collins AR. GIS-based multi-criteria decision analysis of utility-scale wind farm site suitability in West Virginia. Geo J. 2022; 87(5): 3735–3757.
24. Ramírez-Rosado IJ, Monteiro C, García-Garrido E, Miranda V, Fernández-Jiménez LA, Zorzano-Santamaría PJ. Negotiation aid system to define priority maps for wind farm development. IEEE Trans Power Syst. 2005; 20(2): 618–626.
25. Burton T, Jenkins N, Sharpe D, Bossanyi E. Wind energy handbook. John Wiley & Sons; 2011.

26. Modi VJ, Fernando MSUK. On the performance of the Savonius wind turbine. J Sol Energy Eng. 1989 Feb; 111: 71–81.
27. Zemamou M, Aggour M, Toumi AJEP. Review of savonius wind turbine design and performance. Energy Procedia. 2017; 141: 383–388.
28. Mikulevicius R, Rozovskii BL. Stochastic Navier--Stokes equations for turbulent flows. SIAM J Math Anal. 2004; 35(5): 1250–1310.
29. Temam R. Navier–Stokes equations and nonlinear functional analysis. Philadelphia: Society for industrial and applied mathematics. 1995.
30. Foias C, Manley O, Rosa R, Temam R. Navier-Stokes equations and turbulence. Vol. 83. Cambridge: Cambridge University Press; 2001.
31. Doering CR, Gibbon JD. Applied analysis of the Navier-Stokes equations (No. 12). Cambridge: Cambridge university press; 1995.
32. Franco JM, Partal P. The Newtonian fluid. Rheology. 2010; 1: 74–95.
33. Ge M, Wu Y, Liu Y, Yang XI. A two-dimensional Jensen model with a Gaussian-shaped velocity deficit. Renew Energy. 2019; 141: 46–56.
34. Shakoor R, Hassan MY, Raheem A, Wu YK. Wake effect modeling: A review of wind farm layout optimization using Jensen′ s model. Renew Sustain Energy Rev. 2016; 58: 1048–1059.
35. Tian L, Zhu W, Shen W, Song Y, Zhao N. Prediction of multi-wake problems using an improved Jensen wake model. Renew Energy. 2017; 102: 457–469.
36. Hallinan Jr AJ. A review of the Weibull distribution. J Qual Technol. 1993; 25(2): 85–93.
37. Lai CD, Murthy DNP, Xie M. Weibull distributions. Wiley Interdiscip Rev: Comput Stat. 2011; 3(3): 282–287.
38. Lai CD, Murthy DN, Xie M. Weibull distributions and their applications. In: Springer handbook of Engineering Statistics. London: Springer; 2006; 63–78.
39. Best DJ, Fisher NI. Efficient simulation of the von Mises distribution. J R Stat Soc: C Appl Stat. 1979; 28(2): 152–157.
40. Gatto R, Jammalamadaka SR. The generalized von Mises distribution. Stat Methodol. 2007; 4(3): 341–353.
41. Carta JA, Ramírez P, Bueno C. A joint probability density function of wind speed and direction for wind energy analysis. Energy Convers Manag. 2008; 49: 1309–1320.
42. Olimpo Anaya-Lara, McMillan David JK, Ding Yiannis L. Offshore Wind Energy: Technology, Innovation and Development. Wiley; 2014.
43. Cortina G, Sharma V, Torres R, Calaf M. Mean kinetic energy distribution in finite-size wind farms: A function of turbines' arrangement. Renew Energy. 2020; 148: 585–599.
44. Cortina G, Calaf M, Cal RB. Distribution of mean kinetic energy around an isolated wind turbine and a characteristic wind turbine of a very large wind farm. Phys Rev Fluids. 2016; 1(7): 074402.
45. Rawn BG, Gibescu M, Kling WL. Kinetic energy from distributed wind farms: Technical potential and implications. In 2010 IEEE PES Innovative Smart Grid Technologies Conference Europe (ISGT Europe). 2010 Oct; 1–8.
46. Rawn BG, Gibescu M, Kling WL. A static analysis method to determine the availability of kinetic energy from wind turbines. In IEEE PES General Meeting. 2010 Jul; 1–8.
47. Jamdade PG, Patil SV, Jamdade SG. Assessment of Power Coefficient of an Offline Wind Turbine Generator System. Electronic Journal of Energy and Environment. 2013; 1(3): 41–48.

